

## **THREE-DIMENSIONAL LOCALIZATION ALGORITHM FOR MIXED NEAR-FIELD AND FAR-FIELD SOURCES BASED ON ESPRIT AND MUSIC METHOD**

**Jiajia Jiang<sup>\*</sup>, Fajie Duan, and Jin Chen**

The State Key Lab of Precision Measuring Technology & Instruments, Tianjin University, Tianjin, China

**Abstract**—A three-dimensional (3-D) source localization algorithm of joint elevation, azimuth angles and range estimation for the mixed near-field (NF) and far-field (FF) sources is presented in this paper. We first estimate the elevation angles of all mixed sources by using the generalized ESPRIT method. With the elevation angle estimates, the range parameters of all mixed sources are obtained, and then both the NF and FF sources are distinguished. Finally, with the elevation angle and range estimates, the azimuth angles of all mixed sources are acquired based on the conventional high-resolution MUSIC method. The proposed algorithm avoids parameter match operation, and requires neither a multidimensional search nor high-order statistics (HOS). Simulation and experiment results show the performance of the proposed algorithm in this paper.

### **1. INTRODUCTION**

Source localization is one of the most important topics in the passive sonar, radar, microphone arrays, and seismic exploration systems [1]. Parameter estimation methods of multiple sources generally assume that all sources are in the FF [2–8] or NF [9–20] of the array. When all sources are in the FF [2–8], each signal received by the array has planar wavefront. For the FF sources scenario, many one-dimensional (1-D) methods [2–5] for estimating azimuth angle have been proposed based on the 1-D linear array, such as 1-D MUSIC algorithm [2] and 1-D ESPRIT algorithm [3]; and then based on some two-dimensional (2-D) arrays, these 1-D estimation methods [2–5] are extended by researches so as to form 2-D methods for estimating the elevation and azimuth angles [6–8].

---

*Received 12 December 2012, Accepted 15 January 2013, Scheduled 21 January 2013*

\* Corresponding author: Jiajia Jiang (tmjiangjiajia@163.com).

However, when a source is in the Fresnel region of the array aperture (see [9] for more details), the plane-wave approximation to the spherical wave-fronts is no more valid and a more accurate approximation is required. The wave-front shape varies nonlinearly with the array position and is characterized by both the azimuth angle and the range parameters of the source. For the NF sources scenario, many 2-D parameters (azimuth angle and range) estimation methods [9–12] have been also presented based on the 1-D linear array, and then corresponding three-dimensional (3-D) parameters (elevation and azimuth angles and range) estimation methods [13–20] have been also developed.

Generally, most of FF source localization algorithms [2–8] assume that all sources are the pure FF ones, and most of NF source localization algorithms [9–20] assume that all sources are the pure NF ones. However, in some practical applications, the NF sources and FF sources may coexist, such as speaker localization using microphone arrays or acoustic source localization using sonar arrays [21–23]. If so, the above-mentioned algorithms [2–20], which are designed to locate the pure FF sources or pure NF sources, may fail to locate the mixed sources [21–23]. To solve the localization issue of the mixed NF and FF sources, recently, a two-stage MUSIC (TSM) algorithm [21], based on the HOS, is presented. However, for requiring HOS and spectral peak search, the TSM algorithm has a higher computational burden. In order to reduce the computational cost, He et al. present a 1-D MUSIC-based localization (1-DML) algorithm [22]. Nevertheless, when estimating the parameters (elevation angle and range) of the NF sources, the 1-DML algorithm [22] obtains lower azimuth angle estimation performance than the TSM algorithm [21]. In addition, Wang et al. also propose a sparse signal reconstruction-based localization (SSRL) algorithm [23], and the SSRL algorithm gains better estimation performance than the TSM algorithm.

TSM algorithm [21], 1-DML algorithm [22] and SSRL algorithm [23] are the outstanding contribution in the area of the mixed NF and FF sources localization. However, these localization algorithms [21–23] for the mixed NF and FF sources scenario are only based on the uniform linear array (ULA), and thus are only able to estimate 1-D parameter (azimuth angle) for the FF sources and 2-D parameters (azimuth angle and range) for the NF sources [21–23]. Up to now, the relevant paper about 3-D parameters (elevation, azimuth angles and range) estimation of the mixed NF and FF sources is very rare. Therefore, in this paper, based on the ESPRIT and MUSIC methods and by employing a crossed array, a 3-D mixed NF and FF sources localization algorithm is proposed. The proposed algorithm

is based on the second-order statistics (SOS) and requires only 1-D search, therefore it has low computational burden. At the same time, the proposed algorithm is able to avoid parameter pairing procedure.

The following notations will be used throughout. Superscripts  $T$  and  $H$  represent the transpose and conjugate transpose, respectively, while  $\text{diag}\{\cdot\}$ ,  $\arg(\cdot)$  and  $\det\{\cdot\}$  define a diagonal matrix, calculates phase and calculates determinant, respectively.

### 2. 3-D MIXED SIGNAL MODEL

Consider  $K$  narrowband independent radiating sources  $s_k(t)$ ,  $1 \leq k \leq K$ , generated by the mixed NF and FF sources, impinging on a crossed array placed in the  $X$ - $Z$  plane (Fig. 1), and assume that the first  $K_1$  sources are the FF sources (other  $K - K_1$  sources are the NF sources). Each uniform linear array (ULA) branch consists of  $2M + 1$  uniformly spaced omni-directional sensors with interelement spacing  $d$ .

Let the center of array be the phase reference point. The ULA output aligned with the  $X$  and  $Z$  axes are expressed [16, 17] respectively as

$$\mathbf{X}(t) = \sum_{k=1}^K \mathbf{a}(\theta_k, \varphi_k, r_k) s_k(t) + \mathbf{N}_x(t) = \mathbf{A}(\theta, \varphi, r) \mathbf{S}(t) + \mathbf{N}_x(t) \quad (1)$$

$$\mathbf{Z}(t) = \sum_{k=1}^K \mathbf{b}(\theta_k, r_k) s_k(t) + \mathbf{N}_z(t) = \mathbf{B}(\theta, r) \mathbf{S}(t) + \mathbf{N}_z(t) \quad (2)$$

where both  $\mathbf{X}(t) = [x_{-M}(t), x_{-M+1}(t), \dots, x_0(t), \dots, x_M(t)]^T$  and  $\mathbf{Z}(t) = [z_{-M}(t), z_{-M+1}(t), \dots, z_0(t), \dots, z_M(t)]^T$  are  $(2M + 1) \times 1$

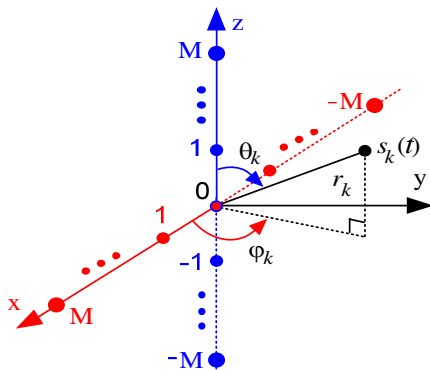


Figure 1. The crossed array configuration.

array output vectors.  $\mathbf{S}(t) = [s_1(t), \dots, s_k(t), \dots, s_K(t)]^T$  is the  $K \times 1$  mixed NF and FF sources vector. Both  $\mathbf{N}_x(t)$  and  $\mathbf{N}_z(t)$  represent the  $(2M + 1) \times 1$  noise vectors.  $\mathbf{A}(\theta, \varphi, r)$  represents the 3-D manifold matrix of the mixed NF and FF sources, which is given [16, 17] by

$$\mathbf{A}(\theta, \varphi, r) = [\mathbf{a}(\theta_1, \varphi_1, r_1), \mathbf{a}(\theta_2, \varphi_2, r_2), \dots, \mathbf{a}(\theta_K, \varphi_K, r_K)] \quad (3)$$

$$\mathbf{a}(\theta_k, \varphi_k, r_k) = \left[ e^{j[(-M)\alpha_{xk} + (-M)^2\beta_{xk}]}, e^{j[(-M+1)\alpha_{xk} + (-M+1)^2\beta_{xk}]}, \dots, e^{j[m\alpha_{xk} + m^2\beta_{xk}]}, \dots, e^{j[M\alpha_{xk} + M^2\beta_{xk}]} \right]^T \quad (4)$$

$$\alpha_{xk} = -2\pi \frac{d}{\lambda} \sin \theta_k \cos \varphi_k \quad (5)$$

$$\beta_{xk} = \pi \frac{d^2}{\lambda r_k} (1 - \sin^2 \theta_k \cos^2 \varphi_k) \quad (6)$$

where  $\lambda$  is the wavelength of sources.  $d \leq \lambda/4$  [9–12] is the distance between two adjacent sensors.  $\theta_k \in [0, \pi]$ ,  $\varphi_k \in [0, \pi]$  and  $r_k \in [0.62(D^3/\lambda)^{1/2}, +\infty)$  [24] with  $D$  representing the array aperture denote the elevation angle, azimuth angles and range of the  $k$ -th source, respectively. And  $\mathbf{B}(\theta, r)$  represents the 2-D manifold matrix of the mixed NF and FF sources, which is expressed [21] as

$$\mathbf{B}(\theta, r) = [\mathbf{b}(\theta_1, r_1), \mathbf{b}(\theta_2, r_2), \dots, \mathbf{b}(\theta_K, r_K)] \quad (7)$$

$$\mathbf{b}(\theta_k, r_k) = \left[ e^{j[(-M)\alpha_{zk} + (-M)^2\beta_{zk}]}, e^{j[(-M+1)\alpha_{zk} + (-M+1)^2\beta_{zk}]}, \dots, e^{j[m\alpha_{zk} + m^2\beta_{zk}]}, \dots, e^{j[M\alpha_{zk} + M^2\beta_{zk}]} \right]^T \quad (8)$$

$$\alpha_{zk} = -2\pi \frac{d}{\lambda} \cos \theta_k \quad (9)$$

$$\beta_{zk} = \pi \frac{d^2}{\lambda r_k} \sin^2 \theta_k \quad (10)$$

Note that, when the  $k$ -th source is a FF source,  $\{\beta_{xk}, \beta_{zk}\}$  are approximated by zero due to farther range of FF source (see [21, 22] in detail). Therefore, the FF source can be considered as the special NF one, and the steering vector of any one source (NF or FF source) can be expressed by (4) or (8).

Throughout the paper, the following assumptions are assumed to hold: 1) The number of sources is known or correctly estimated by the minimum description length (MDL) detection criterion or the Akaike information criterion (AIC) [25]; 2) The incoming source signals are statistically independent, zero-mean complex Gaussian random processes; 3) The noise is zero-mean, complex circular Gaussian, and spatially uniformly white, and is statistically independent of all the

signals; 4) Before localizing the sources, the array errors, such as gain and phase errors, position errors and mutual coupling errors etc., have been calibrated through relevant array errors calibration method as [1–25].

### 3. PROPOSED ALGORITHM

#### 3.1. Estimate the Elevation of All NF and FF Sources

From (2), one can observe that the ULA output  $\mathbf{Z}(t)$  aligned with the  $Z$  axes only contains both the elevation angle and range parameters. We divide the ULA aligned with the  $Z$  axes into two subarrays. The first subarray comprises the first  $2M$  sensors, while the second one comprises the last  $2M$  sensors (inverse order). The signal output of the two subarrays can be given respectively by

$$\begin{aligned} \mathbf{Z}_1(t) &= [z_{-M}(t), z_{-M+1}(t), \dots, z_0(t), \dots, z_{M-1}(t)]^T \\ &= \mathbf{B}_1(\theta, r)\mathbf{S}(t) + \mathbf{N}_{z1}(t) \end{aligned} \quad (11)$$

$$\begin{aligned} \mathbf{Z}_2(t) &= [z_M(t), z_{M-1}(t), \dots, z_0(t), \dots, z_{-(M-1)}(t)]^T \\ &= \mathbf{B}_2(\theta, r)\mathbf{S}(t) + \mathbf{N}_{z2}(t) \end{aligned} \quad (12)$$

$$\mathbf{B}_1(\theta, r) = [\mathbf{b}_1(\theta_1, r_1), \mathbf{b}_1(\theta_2, r_2), \dots, \mathbf{b}_1(\theta_K, r_K)] \quad (13)$$

where the matrix  $\mathbf{B}_1(\theta, r)$  is the first  $2M$  rows of the matrix  $\mathbf{B}(\theta, r)$  and  $\mathbf{B}_2(\theta, r)$  is constructed with the last  $2M$  rows of  $\mathbf{B}(\theta, r)$  in reverse order. Both  $\mathbf{N}_{z1}(t) = [n_{-M}(t), \dots, n_0(t), \dots, n_{M-1}(t)]^T$  and  $\mathbf{N}_{z2}(t) = [n_M(t), \dots, n_0(t), \dots, n_{-(M-1)}(t)]^T$  are the subarray noise vectors. The relationship between  $\mathbf{B}_1(\theta, r)$  and  $\mathbf{B}_2(\theta, r)$  can be written as

$$\mathbf{B}_2(\theta, r) = [\mathbf{G}(\theta_1)\mathbf{b}_1(\theta_1, r_1), \dots, \mathbf{G}(\theta_K)\mathbf{b}_1(\theta_K, r_K)] \quad (14)$$

where

$$\mathbf{G}(\theta_k) = \text{diag} \left\{ e^{j2\alpha_{zk}M}, e^{j2\alpha_{zk}(M-1)}, \dots, e^{j2\alpha_{zk}(-M+1)} \right\} \quad (15)$$

Note that  $\mathbf{G}(\theta_k)$  only contains the elevation angle information.

And the relationship between  $\mathbf{B}(\theta, r)$  and  $\mathbf{B}_1(\theta, r)$ ,  $\mathbf{B}_2(\theta, r)$  can be expressed as

$$\mathbf{B}(\theta, r) = \begin{bmatrix} \mathbf{B}_1(\theta, r) \\ \text{last row of } \mathbf{B}(\theta, r) \end{bmatrix} = \begin{bmatrix} \text{first row of } \mathbf{B}(\theta, r) \\ \mathbf{J}\mathbf{B}_2(\theta, r) \end{bmatrix} \quad (16)$$

where  $\mathbf{J}$  is a  $2M \times 2M$  matrix having 1's along the anti-diagonal, and  $\mathbf{J}^2 = \mathbf{I}$ .

Eigendecompose the array covariance matrix  $\mathbf{R}_z = E\{\mathbf{Z}(t)\mathbf{Z}^H(t)\}$  to construct a  $(2M + 1) \times K$  signal-subspace matrix  $\mathbf{U}_s$  whose columns

are the  $(2M + 1) \times 1$  eigenvectors associated with the  $K$  largest eigenvalues of  $\mathbf{R}_z$ , and  $(2M + 1) \times (2M + 1 - K)$  noise-subspace matrix  $\mathbf{U}_n$  whose columns are the  $(2M + 1) \times 1$  eigenvectors associated with the  $(2M + 1 - K)$  smallest eigenvalues of  $\mathbf{R}_z$ . Based on the ESPRIT method, there exists a  $K \times K$  full-rank matrix  $\mathbf{T}$  satisfying  $\mathbf{U}_s = \mathbf{B}(\theta, r)\mathbf{T}$ . Therefore,  $\mathbf{U}_s$  can be rewritten as

$$\begin{aligned} \mathbf{U}_s &= \begin{bmatrix} \mathbf{U}_{s1} \\ \text{last row of } \mathbf{U}_s \end{bmatrix} = \begin{bmatrix} \text{first row of } \mathbf{U}_s \\ \mathbf{U}_{s2} \end{bmatrix} = \mathbf{B}(\theta, r)\mathbf{T} \\ &= \begin{bmatrix} \mathbf{B}_1(\theta, r) \\ \text{last row of } \mathbf{B}(\theta, r) \end{bmatrix} \mathbf{T} = \begin{bmatrix} \text{first row of } \mathbf{B}(\theta, r) \\ \mathbf{JB}_2(\theta, r) \end{bmatrix} \mathbf{T} \\ &\Rightarrow \begin{cases} \mathbf{U}_{s1} = \mathbf{B}_1(\theta, r)\mathbf{T} \\ \mathbf{U}_{s2} = \mathbf{JB}_2(\theta, r)\mathbf{T} \end{cases} \end{aligned} \quad (17)$$

where  $\mathbf{U}_{s1}$  is the first  $2M$  rows of the signal-subspace  $\mathbf{U}_s$ , while  $\mathbf{U}_{s2}$  is the last  $2M$  rows of the signal-subspace  $\mathbf{U}_s$ .

Similar to the generalized ESPRIT method [4] for 1-D elevation angle estimation, we define a matrix

$$\begin{aligned} &\Phi(\theta)\mathbf{U}_{s1} - \mathbf{JU}_{s2} \\ &= [\Phi(\theta)\mathbf{B}_1(\theta, r) - \mathbf{B}_2(\theta, r)]\mathbf{T} = [(\Phi(\theta) - \mathbf{G}(\theta_1))\mathbf{b}_1(\theta_1, r_1), \\ &\quad \dots, (\Phi(\theta) - \mathbf{G}(\theta_K))\mathbf{b}_1(\theta_K, r_K)]\mathbf{T} \end{aligned} \quad (18)$$

where  $\Phi(\theta) = \text{diag}\{e^{j2\alpha_z M}, e^{j2\alpha_z(M-1)}, \dots, e^{j2\alpha_z(-M+1)}\}$ .

From (18), we can observe that the  $k$ -th column of the matrix  $\Phi(\theta)\mathbf{B}_1(\theta, r) - \mathbf{B}_2(\theta, r)$  becomes equal to zero when  $\theta = \theta_k$ . In such a case, the matrix  $\Phi(\theta)\mathbf{U}_{s1} - \mathbf{JU}_{s2}$  will drop rank. Furthermore, we can obtain the elevation angle estimates as when the matrix  $\mathbf{U}_{s1}^H \Phi(\theta)\mathbf{U}_{s1} - \mathbf{U}_{s1}^H \mathbf{JU}_{s2}$  [4] drops rank for the values of  $\theta_k$ ,  $k = 1, \dots, K$ . Therefore, the following spectral function can be used to find  $\theta_k$ ,  $k = 1, \dots, K$ :

$$P(\theta) = 1 / \det \left\{ \mathbf{U}_{s1}^H [\Phi(\theta)\mathbf{U}_{s1} - \mathbf{JU}_{s2}] \right\} \quad (19)$$

By means of only 1-D search over  $\theta$ , the estimates  $\hat{\theta}_k$ ,  $k = 1, \dots, K$  of the elevation angles  $\theta_k$ ,  $k = 1, \dots, K$  of all NF and FF sources can be obtained.

### 3.2. Estimate Range Parameters of All NF and FF Sources and Distinguish NF Sources from the Mixed Sources

Based on the MUSIC method [2], a 2-D MUSIC spectrum function can be given by

$$P(\theta, r) = 1 / \left[ \mathbf{b}^H(\theta, r)\mathbf{U}_n\mathbf{U}_n^H\mathbf{b}(\theta, r) \right] \quad (20)$$

Since the elevation angle estimates  $\hat{\theta}_k, k = 1, \dots, K$  of all NF and FF sources have been obtained in Section 3.1, (20) can be rewritten as

$$P(r) = 1/\left[\mathbf{b}^H\left(\hat{\theta}_k, r\right)\mathbf{U}_n\mathbf{U}_n^H\mathbf{b}\left(\hat{\theta}_k, r\right)\right], \quad k = 1, 2, \dots, K \quad (21)$$

Based on (8), we define  $\mathbf{b}(\theta_k, r)$  as

$$\mathbf{b}(\theta_k, r) = \boldsymbol{\gamma}_k(r)\mathbf{v}_k \quad (22)$$

where

$$\boldsymbol{\gamma}_k(r) = \text{diag}\left\{e^{j(-M)^2\beta_{zk}}, e^{j(-M+1)^2\beta_{zk}}, \dots, e^{j(M)^2\beta_{zk}}\right\} \quad (23)$$

$$\beta_{zk}(r) = \pi \frac{d^2}{\lambda r} \sin^2(\theta_k) \quad (24)$$

$$\mathbf{v}_k = \left[e^{j(-M)\alpha_{zk}}, \dots, e^{jm\alpha_{zk}}, \dots, e^{jM\alpha_{zk}}\right]^T \quad (25)$$

As [26, 27], we denote  $z = e^{j\beta_{zk}}$ , and then (23) can be rewritten as

$$\boldsymbol{\gamma}_k(z) = \text{diag}\left\{z^{(-M)^2}, z^{(-M+1)^2}, \dots, z^{(M)^2}\right\} \quad (26)$$

Similar to the Root MUSIC method [26, 27], the denominator of function (21) can be rewritten as the following polynomial:

$$g^k(z) = \mathbf{v}_k^H \boldsymbol{\gamma}_k^H(1/z) \mathbf{U}_n \mathbf{U}_n^H \boldsymbol{\gamma}_k(z) \mathbf{v}_k, \quad k = 1, \dots, K \quad (27)$$

With the elevation angle estimates  $\hat{\theta}_k, k = 1, \dots, K$ , we can obtain  $L(L \geq 1)$  closest to the unit circle roots  $z_i^k, i = 1, \dots, L$  of  $g^k(z)$  by substituting each  $\hat{\theta}_k$  back into (27).

Further, if  $L = 1$ , that is to say, when there exists only one closest to the unit circle roots  $z_i^k, i = 1 = L$  of  $g^k(z)$ , we can determine that there exists only one source at  $\theta_k$  direction.

If  $L = 2$ , that is to say, when there exist two roots which are closest to the unit circle,  $z_i^k, i = 1, 2$  of  $g^k(z)$ , we can determine that there exist two sources at  $\theta_k$  direction (that is to say, the two signal sources have the same elevation angle). Therefore, we can easily determine how many sources exist at the same direction.

Then, based on  $z = e^{j\beta_{zk}}$ , we can obtain the range estimates  $\hat{r}_k$  of range  $r_k$ :

$$\hat{r}_k = \frac{\pi d^2 \sin^2\left(\hat{\theta}_k\right)}{\lambda \cdot \arg\left(z_i^k\right)}, \quad i = 1, \dots, L \quad (28)$$

when  $\hat{r}_k \in [0.62(D^3/\lambda)^{1/2}, 2D^2/\lambda]$  (Fresnel region [24]), the source  $s_k(t)$  corresponding to  $\hat{r}_k$  is a NF source. On the contrary, when  $\hat{r}_k \in (2D^2/\lambda, +\infty)$ , the source  $s_k(t)$  corresponding to  $\hat{r}_k$  is a FF source. Thus, we can easily distinguish whether the source is NF or FF one.

### 3.3. Estimate Azimuth Angles of All NF and FF Sources

From (1), we can see that  $\mathbf{X}(t)$  contains 3-D parameters, namely elevation, azimuth angles and range. The eigendecomposition of the covariance matrix  $\mathbf{R}_x = E\{\mathbf{X}(t)\mathbf{X}^H(t)\}$  can be written as

$$\mathbf{R}_x = \bar{\mathbf{U}}_s \Lambda_s \bar{\mathbf{U}}_s^H + \bar{\mathbf{U}}_n \Lambda_n \bar{\mathbf{U}}_n^H \quad (29)$$

where  $\Lambda_s$  and  $\Lambda_n$  are the diagonal matrices that contain the signal- and noise-subspace eigenvalues of  $\mathbf{R}_x$ , respectively, whereas  $\bar{\mathbf{U}}_s$  and  $\bar{\mathbf{U}}_n$  are the orthonormal matrices that contain the signal- and noise-subspace eigenvectors of  $\mathbf{R}_x$ , respectively. Based on the MUSIC method, a 3-D MUSIC pseudo-spectrum scalar function is given by:

$$P(\theta, \varphi, r) = 1/\left[\mathbf{a}^H(\theta, \varphi, r)\bar{\mathbf{U}}_n\bar{\mathbf{U}}_n^H\mathbf{a}(\theta, \varphi, r)\right] \quad (30)$$

With the elevation angle and range estimates  $\{\hat{\theta}_k, \hat{r}_k\}$ ,  $k = 1, \dots, K$ , (30) can be rewritten as

$$P(\varphi) = 1/\left[\mathbf{a}^H(\hat{\theta}_k, \varphi, \hat{r}_k)\bar{\mathbf{U}}_n\bar{\mathbf{U}}_n^H\mathbf{a}(\hat{\theta}_k, \varphi, \hat{r}_k)\right], \quad k = 1, \dots, K \quad (31)$$

By means of only 1-D search over  $\varphi$ , the estimates  $\hat{\varphi}_k$ ,  $k = 1, \dots, K$  of the azimuth angles  $\varphi_k$ ,  $k = 1, \dots, K$  of all NF and FF sources can be obtained.

### 3.4. Summary of the Proposed Algorithm

The proposed algorithm can be described as follows:

- Step 1:** Obtain the estimate  $\hat{\mathbf{R}}_z = (1/N)\sum_{n=1}^N \mathbf{Z}(t)\mathbf{Z}^H(t)$  of the covariance matrix  $\mathbf{R}_z$ , and then implement the eigendecomposition of  $\hat{\mathbf{R}}_z$  to obtain  $\mathbf{U}_s$  and  $\mathbf{U}_n$ , where  $N$  is the number of snapshots;
- Step 2:** Based on the generalized ESPRIT method, obtain the estimates  $\hat{\theta}_k$ ,  $k = 1, \dots, K$  of the elevation angles  $\theta_k$ ,  $k = 1, \dots, K$  of all NF and FF sources from (19);
- Step 3:** Similar to the Root MUSIC method, with the elevation angle estimates  $\hat{\theta}_k$ ,  $k = 1, \dots, K$ , achieve the estimation of the range parameters of all NF and FF sources from (28), and then distinguish the NF and FF sources according to the size of the range parameters of sources;
- Step 4:** Obtain the estimate  $\hat{\mathbf{R}}_x = (1/N)\sum_{n=1}^N \mathbf{X}(t)\mathbf{X}^H(t)$  of the covariance matrix  $\mathbf{R}_x$ , and then implement the eigendecomposition of  $\mathbf{R}_x$  so as to obtain  $\bar{\mathbf{U}}_n$ ;

**Step 5:** With the elevation angle and range estimates  $\{\hat{\theta}_k, \hat{r}_k\}$ ,  $k = 1, \dots, K$ , estimate the azimuth angles  $\hat{\varphi}_k$ ,  $k = 1, \dots, K$  from (31).

### 3.5. Discussion

In this section, when estimating the elevation angle and range parameters, the proposed algorithm is compared with both the TSM algorithm [21] and 1-DML algorithm [22] in two aspects: Estimation accuracy and Computational complexity. And then we analyze the performance of the proposed algorithm in other two aspects: Parameter pairing and Number of dimensions.

**Estimation accuracy:** in [22], when estimating the elevation angle of FF sources, 1-DML algorithm is able to locate  $2M$  sources using a ULA of  $(2M + 1)$  sensors by means of the conventional MUSIC method, while the NF estimator (see Equation (23) in [22]) of 1-DML algorithm is only able to locate  $M$  sources using a ULA of  $(2M + 1)$  sensors. So eventually 1-DML algorithm is only able to locate  $M$  mixed sources using a ULA of  $(2M + 1)$  sensors. And when estimating the elevation angle of NF sources, 1-DML algorithm only utilizes part of the (anti-diagonal) information of the covariance matrix. However, by using the generalized ESPRIT method, the proposed algorithm can locate  $(2M - 1)$  sources using a ULA (aligned with the  $Z$  axes) of  $(2M + 1)$  sensors and makes full use of all information of  $\mathbf{R}_z$ . Therefore, the proposed algorithm is able to locate more sources than 1-DML algorithm, and it is expected that for estimating the elevation angle of NF sources, the proposed algorithm can gain better estimation performance than 1-DML algorithm. In addition, when estimating the range parameters, the proposed algorithm utilize Root MUSIC-Like method (see Equation (27)) to estimate the range parameters of the mixed sources. This indicates that the proposed algorithm can obtain better range parameter estimation accuracy than 1-DML algorithm according to the results of [26].

**Computational complexity:** in this discussion, we only consider the major computations. In [21], the HOS-based TSM algorithm is computationally inefficient, compared with the SOS-based 1-DML algorithm. Furthermore, to obtain the elevation angle estimates of mixed NF and FF sources, 1-DML algorithm needs to form one  $(2M + 1) \times (2M + 1)$  and one  $(2M + 2 - T) \times (2M + 2 - T)$  matrices, to perform eigendecompositions of the two matrices, and to execute twice one-dimensional MUSIC spectral search, where  $T$  denotes the number of overlapping subvectors (see Equation (18) in [22]). Moreover, 1-DML algorithm executes  $K - K_1$  times one-dimensional MUSIC spectral search so as to obtain the estimates of the range parameter.

However, to estimate the elevation angles of the mixed NF and FF sources, the proposed algorithm only needs to form one  $(2M + 1) \times (2M + 1)$  matrix, to perform eigendecomposition of the matrix, and to execute once one-dimensional search. Moreover, the proposed algorithm executes  $K$  times root-polynomial construction and solution for range parameter estimation, which is less computational cost than the MUSIC method according to [26, 27]. From the analysis above, it is obvious that the proposed algorithm gains less computational cost than both the TSM algorithm and 1-DML algorithm when estimating both the elevation angle and range parameters. In addition, for estimating the azimuth angle, the proposed algorithm also needs to form another  $(2M + 1) \times (2M + 1)$  matrix, to perform eigendecomposition of the matrix, and to execute one-dimensional search.

**Parameter pairing:** many 2-D estimation algorithms [5–8] for the pure FF sources and 3-D estimation algorithms [14, 16, 17] for the pure NF sources need to pair parameters so as to achieve the source localization. The failure in pairing will cause severe performance degradation. However, the proposed algorithm first estimates the elevation angle  $\hat{\theta}_k$ , then with the elevation angle estimate  $\hat{\theta}_k$  obtains the range estimate  $\hat{r}_k$ , and last obtains the estimate  $\hat{\varphi}_k$  with the estimate  $\{\hat{\theta}_k, \hat{r}_k\}$ . Therefore, the proposed algorithm avoids parameter match operation.

**Number of dimensions:** until now, many 1-D elevation angle estimation algorithms [2–4] for the pure FF sources, 2-D elevation and azimuth angles estimation algorithms [5–8] for the pure FF sources, 2-D azimuth angle and range estimation algorithms [9–12] for the pure NF sources, 3-D elevation, azimuth angles and range estimation algorithms [13–20] for the pure NF sources, and 2-D azimuth angle and range estimation algorithms [21–23] for the mixed NF and FF sources are proposed. However, by now, the relevant paper about 3-D parameters (elevation, azimuth angles and range) estimation of the mixed NF and FF sources is very rare. Therefore, based on ESPRIT and MUSIC methods, we present a 3D localization algorithm of the mixed NF and FF sources so as to solve the 3D localization issue of the mixed sources.

#### 4. SIMULATIONS AND EXPERIMENT

In this section, to verify the performance of the proposed algorithm, without loss of generality, we consider a crossed array placed in the  $X$ - $Z$  plane, and each ULA branch consists of 7 ( $M = 3$ ) uniformly spaced omni-directional sensors with a quarter-wavelength inter-sensor spacing. In the following each experiment, the performances of

all mentioned algorithms are measured by the estimated root-mean-square error (RMSE) [28, 29] of 500 independent Monte Carlo [30, 31] experiments. For comparison, when estimating the elevation angle and range parameters, we simultaneously execute 1-DML algorithm. Note that 1-DML algorithm uses the same ULA aligned with the  $Z$  axes with the proposed algorithm. In addition, the related CRLBs [21, 22, 32, 33] are given in the following relevant figures. Note that as [34], the estimation performance of the range parameter is only for NF source in the following each experiment, and we would not give the estimation performance of the range parameter of FF source although the range parameter of FF source can be obtained by (28).

#### 4.1. Pure NF Sources

In the *first* experiment, a pure NF source case that the two NF sources have different elevations, azimuth angles and range parameters is considered. The two sources are located at  $\{\theta_1 = 70^\circ, r_1 = 2.3\lambda, \varphi_1 = 40^\circ\}$  and  $\{\theta_2 = 120^\circ, r_2 = 1.6\lambda, \varphi_2 = 50^\circ\}$ , respectively. The snapshot number is set equal to 600 and signal-to-noise ratio (SNR) varies from 0 dB to 30 dB. From Figs. 2 and 3, it can be seen that the proposed algorithm has much better elevation angle and range estimation performance than 1-DML algorithm, which is consistent with the analysis given in Section 3-Discussion. Moreover, the RMSEs of the range estimation for the second source, which is closer to the array, are smaller than that of the first source. From Fig. 4, one can see that with high SNRs, the azimuth angle estimation performance of the proposed algorithm is reasonably close to the deterministic CRLB. In addition, from Figs. 2, 3 and 4, one can find that the elevation angle estimation accuracy of the proposed algorithm is higher than its range estimation accuracy, and further its range estimation accuracy is superior to its azimuth angle estimation accuracy. This is because the range estimates are based on the elevation angle ones, and the elevation angle estimates are based on the range ones.

#### 4.2. Mixed NF and FF Sources

In the *second* experiment, a general case that one NF source and one FF source coexist and have the different elevation and azimuth angles, is considered. The two sources are located at  $\{\theta_1 = 110^\circ, r_1 = 1.2\lambda, \varphi_1 = 45^\circ\}$  and  $\{\theta_2 = 60^\circ, r_2 = \infty, \varphi_2 = 25^\circ\}$ , respectively. The snapshot number is set equal to 400 and SNR varies from 0 dB to 30 dB. The simulation results are presented in Figs. 5, 6 and 7. Fig. 5 shows that the proposed method has much better performance than 1-DML algorithm for the elevation angle estimation of NF sources, and

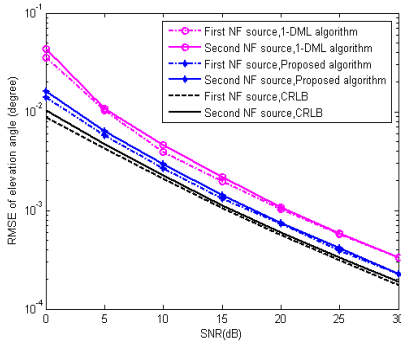


**Figure 2.** RMSEs of elevation angle estimates for pure NF sources versus SNR.

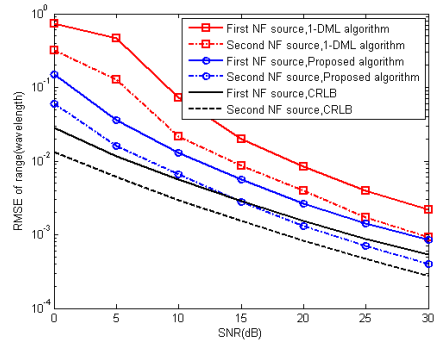


**Figure 3.** RMSEs of range estimates for pure NF sources versus SNR.

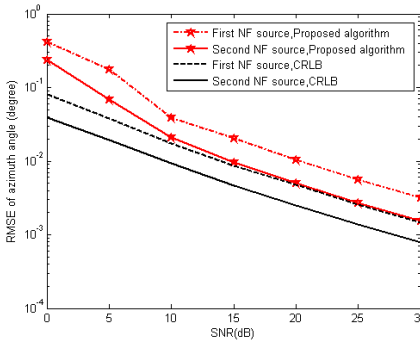


**Figure 4.** RMSEs of azimuth angle estimates for pure NF sources versus SNR.

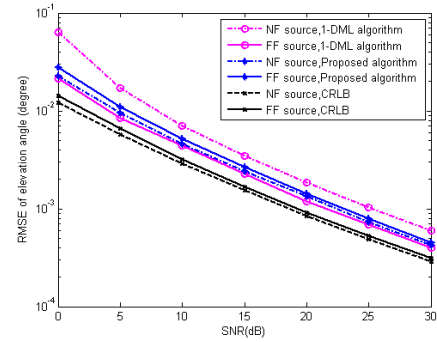


**Figure 5.** RMSEs of elevation angle estimates for mixed sources versus SNR.

they have approximate RMSE for the elevation angle estimation of FF sources. It can be observed from Fig. 6 that the range estimation performance of the proposed algorithm is superior to 1-DML algorithm. Moreover, Fig. 7 shows the RMSE of the azimuth angle estimates of both the NF and FF sources.

### 4.3. Pure FF Sources

In the *third* experiment, a pure FF source case that two sources are located at  $\{\theta_1 = 120^\circ, r_1 = \infty, \varphi_1 = 130^\circ\}$  and  $\{\theta_2 = 60^\circ, r_2 = \infty, \varphi_2 = 50^\circ\}$  respectively, is considered. The snapshot number is set equal to 800 and SNR varies from 0 dB to 30 dB. From Fig. 8, it

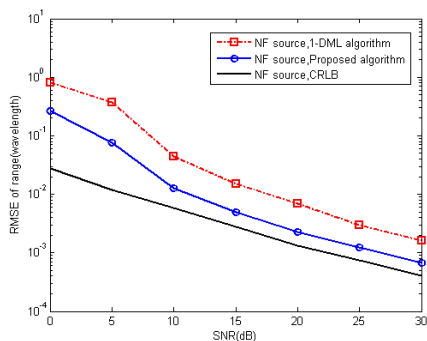


**Figure 6.** RMSEs of range estimates for mixed sources versus SNR.

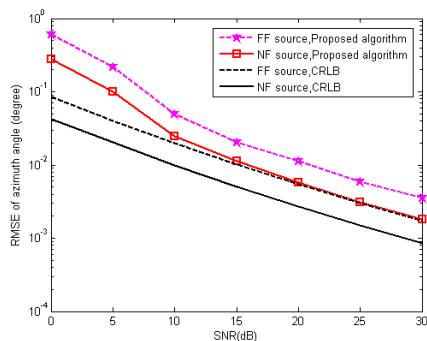


**Figure 7.** RMSEs of azimuth angle estimates for mixed sources versus SNR.

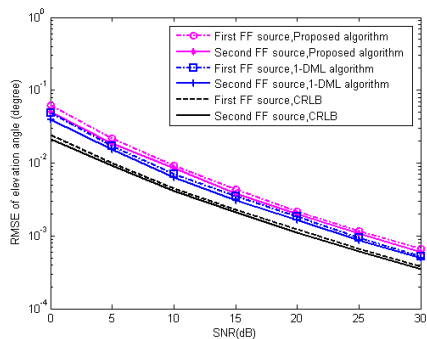


**Figure 8.** RMSEs of elevation angle estimates for pure FF sources versus SNR.

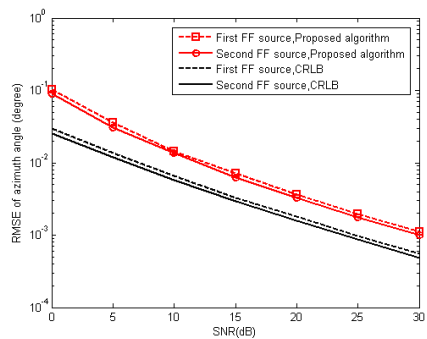


**Figure 9.** RMSEs of azimuth angle estimates for pure FF sources versus SNR.

can be seen that the proposed algorithm has approximated estimation accuracy with 1-DML algorithm. Moreover, one can know from Fig. 9 that RMSEs of the azimuth angle estimates of the two FF sources are approximate. In addition, as it is expected, when SNR increases, the RMSEs of the elevation and azimuth angle estimates decrease and approach to the CRLB.

#### 4.4. Resolution

In the *fourth* experiment, we examine the performance of the proposed algorithm when the angles of sources are close to the horizon, and simultaneously examine that of the angle resolution, by using a united simulation experiment. We consider two NF sources which are located

at  $\{\theta_1 = 90^\circ, r_1 = 1.5\lambda, \varphi_1 = 145^\circ\}$  and  $\{\theta_2 = 90^\circ + \rho_1\theta, r_2 = 1.5\lambda, \varphi_2 = 145^\circ\}$ , with  $\rho_1\theta$  varying in the range  $[-10^\circ, 10^\circ]$  by steps of  $2^\circ$ . It is obvious from the definition of elevation angle (see Fig. 1) that the elevation angle of the first source is in the horizon and the elevation angle of the second source varies around the horizon. SNR is fixed at 5 dB and snapshots number is set to 300. Simulation results are shown in Figs. 10, 11 and 12. From Figs. 10, 11 and 12, we can see that on the one hand, when the elevation angles are close to or in the horizon, both the proposed algorithm and 1-DML algorithm obtain satisfactory elevation, azimuth angle and range estimation accuracy, and further the estimation performance of the proposed algorithm is superior to that of 1-DML algorithm for the estimates of the elevation, azimuth angle and range parameters; on the other hand, both the proposed algorithm and 1-DML algorithm begin to degrade when the elevation angles of the two sources are gradually close to each other, while the 1-DML algorithm degrade more quickly than the proposed algorithm for the estimates of the elevation, azimuth angle and range parameters, which indicates the proposed algorithm has much better elevation, azimuth angle and range resolution than 1-DML algorithm. Note that when the two sources have the same elevation angle, the data covariance matrix is equivalent to obtain double sampling number, and thus both the proposed algorithm and 1-DML algorithm obtain better estimation performance at  $\rho_1\theta = 0$  point than at  $\rho_1\theta \neq 0$  point.

In the *fifth* experiment, we consider two NF sources which are located at  $\{\theta_1 = 80^\circ, r_1 = 1.5\lambda, \varphi_1 = 145^\circ\}$  and  $\{\theta_2 = 70^\circ, r_2 = 1.5\lambda + \rho_2\lambda, \varphi_2 = 145^\circ\}$ , with  $\rho_2\lambda$  varying in the range  $[-0.5\lambda, 0.5\lambda]$  by steps of  $0.1\lambda$ . Let snapshot number and SNR be 300 and 15 dB,

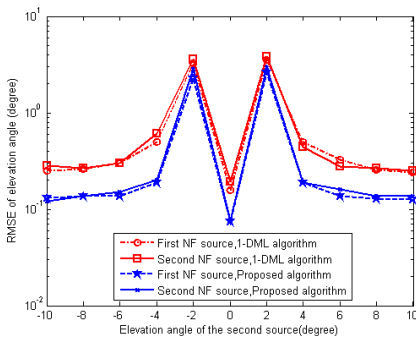


**Figure 10.** The RMSE of elevation angle estimates versus the varied elevation angle of second source.

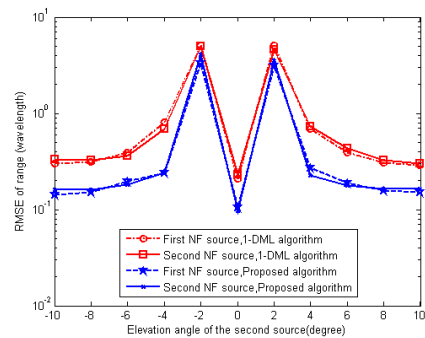


**Figure 11.** The RMSE of range estimates versus the varied elevation angle of second source.

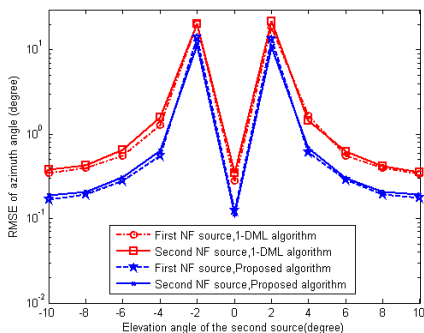


**Figure 12.** The RMSE of azimuth angle estimates versus the varied elevation angle of second source.

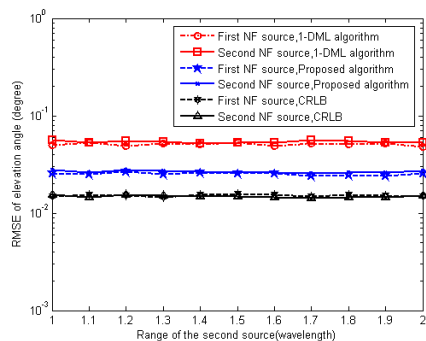


**Figure 13.** The RMSE of elevation angle estimates versus the varied range of second source.

respectively. From Fig. 13, it can be seen that the elevation angle estimates are insensitive to the change of range parameters. It can be observed from Fig. 14 that the range estimates of the first source are also insensitive to the change of the range parameters of the second source. However, when the range of the first source is larger than that of the second source, the RMSEs of the range estimates of the first source is much higher than that of the second source; while when the range of the first source is smaller than that of the second source, the RMSEs of the range estimates of the first source is much lower than that of the second source. Meanwhile, when the two sources have same ranges, the RMSEs of the two range estimates approximates to each other. From Fig. 15, one can see that the changes of RMSEs of azimuth angles are consistent with those of RMSEs of range parameters, because the azimuth angle estimates are based on the range estimates.

In the *sixth* experiment, we consider two NF sources which are located at  $\{\theta_1 = 80^\circ, r_1 = 1.5\lambda, \varphi_1 = 145^\circ\}$  and  $\{\theta_2 = 70^\circ, r_2 = 1.5\lambda, \varphi_2 = 145^\circ + \rho_3\varphi\}$ , with  $\rho_3\varphi$  varying in the range  $[-5^\circ, 5^\circ]$  by steps of  $1^\circ$ . Let snapshot number and SNR be 300 and 15 dB, respectively. It can be seen from Fig. 16 that the azimuth angle estimates are still insensitive to the change of azimuth angle.

In the *seventh* experiment, a special case that two NF sources which are located at  $\{\theta_1 = 65^\circ, r_1 = 2\lambda, \varphi_1 = 30^\circ\}$  and  $\{\theta_2 = 45^\circ, r_2 = 1.5\lambda, \varphi_2 = 45^\circ\}$  respectively and two FF sources which are located at  $\{\theta_3 = 45^\circ, r_3 = \infty, \varphi_3 = 45^\circ\}$  and  $\{\theta_4 = 25^\circ, r_4 = \infty, \varphi_4 = 60^\circ\}$

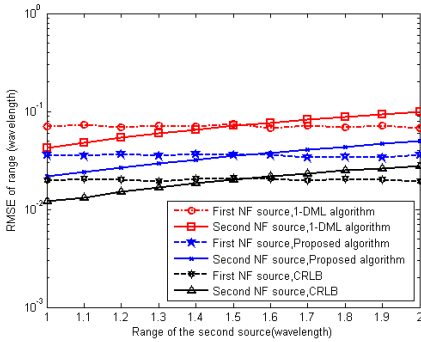


**Figure 14.** The RMSE of range versus the varied range of second source.

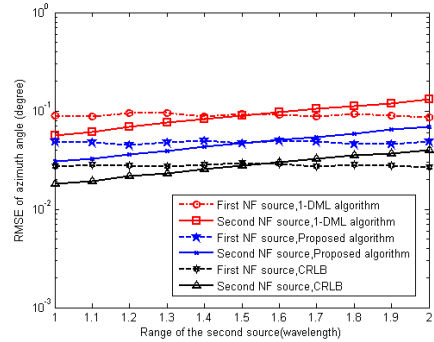


**Figure 15.** The RMSE of azimuth angle versus the varied range of second source.

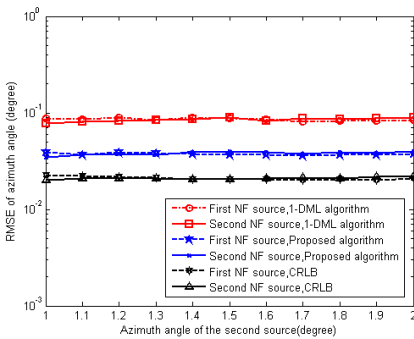


**Figure 16.** The RMSE of azimuth angle versus the varied azimuth angle of second source.

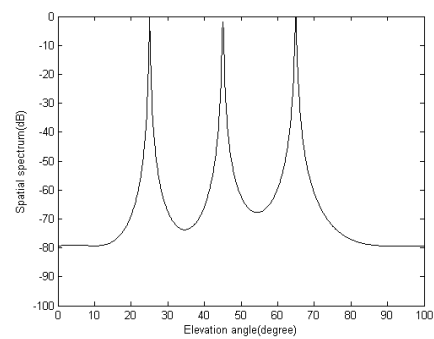


**Figure 17.** The spatial spectrum of elevation angle of the proposed algorithm.

respectively coexist, is considered. Obviously, the second FF source has the same elevation and azimuth angle as the first NF one, namely  $\{\theta_2 = \theta_3, \varphi_2 = \varphi_3\}$ . SNR is set to 20 dB for all these four sources and snapshot number is 500. The simulation results are shown in Figs. 17, 18 and 19. Likewise, in Fig. 18, we filter these roots whose module are below  $R1 = 0.9$  or up  $R3 = 1.1$ ; and with the estimated elevation angle  $\theta_1$  the first time obtained roots of Equation (27) are denoted by circle ( $\circ$ ), with the estimated elevation angle  $\theta_2 = \theta_3$  the second time obtained roots of Equation (27) are denoted by asterisk ( $\times$ ) and with the estimated elevation angle  $\theta_4$  the third time obtained roots of Equation (27) are denoted by plus sign ( $+$ ). From Figs. 17, 18

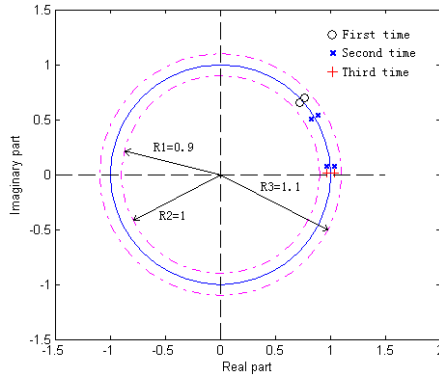


**Figure 18.** The distribution of roots of Equation (27) with the first elevation angle  $\theta_1$  (first time solve Equation (27)), second and third elevation angles  $\theta_2 = \theta_3$  (second time solve Equation (27)) and fourth elevation angle  $\theta_4$  (third time solve Equation (27)).

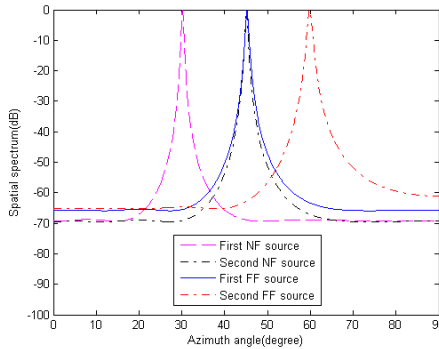


**Figure 19.** The spatial spectrum of azimuth angle of the proposed algorithm.

and 19, one can observe that the proposed algorithm can accurately obtain the elevation and azimuth angle and range parameter estimates. Furthermore, when the ranges of sources are different, all parameters (elevation, azimuth angles and range) can be estimated accurately even though the NF source and FF source have the same elevation and azimuth angles.

### 4.5. Experiment

In this section, we verify the validity of the proposed algorithm experimentally using the in-field data. The data is obtained by

collecting the sine sound wave using the following measurement setup: the experimental setup is shown in Fig. 20. A crossed array is placed in the  $X$ - $Z$  plane, and each ULA branch along  $X$  and  $Z$  axes consists of 5 uniformly spaced omni-directional sound sensors with an  $\lambda/5$  inter-sensor spacing. The total 9 active sound sensors are connected to a data acquisition system (DAS) developed by our project group and placed in a fixed crossed support. The DAS has 9-channel 24-bit analog-to-digital converter module with sample rates of 4 kHz/channel, and the digital data first is collected by a Field Programmable Gate Array (FPGA) and then is transmitted to computer by a Peripheral Component Interconnect (PCI) Card. The sound wave velocity is 340 m/s, and two sound sources which transmit the 680HZ sine wave signal are located at  $\{\theta_1 = 98^\circ, r_1 = 10\lambda, \varphi_1 = 69^\circ\}$  and  $\{\theta_2 = 63.5^\circ, r_2 = \lambda, \varphi_2 = 42^\circ\}$  respectively. According to the definition in Section 2, it is obvious that the Fresnel region of the array is  $0.44\lambda < r < 1.28\lambda$ , and thus the first source is FF one and the second source is NF one. Note that for being far from the array, the FF source is out of the camera and thus can not be seen in Fig. 20. The snapshot number is 500. After the array errors are calibrated, the experiment results are shown in Figs. 21, 22 and 23. Fig. 22 clearly shows the positions of roots of the corresponding sources. Moreover, it can be seen clearly from Figs. 21 and 23 that the elevation angles of the two sources are about  $97.8^\circ$  and  $63.4^\circ$ , respectively, and the azimuth angles of the two sources are about  $68.7^\circ$  and  $42.3^\circ$ , respectively. Note that from the experiment results shown in Figs. 21 and 23, we can see that there exists angle estimation errors  $\{\Delta\theta_1 = 0.2^\circ, \Delta\theta_2 = 0.1^\circ; \Delta\varphi_1 = 0.3^\circ, \Delta\varphi_2 = 0.3^\circ\}$ ,

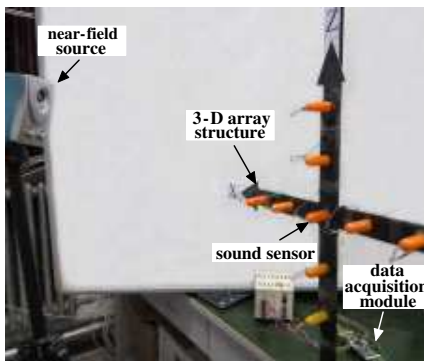


**Figure 20.** Experimental setup.

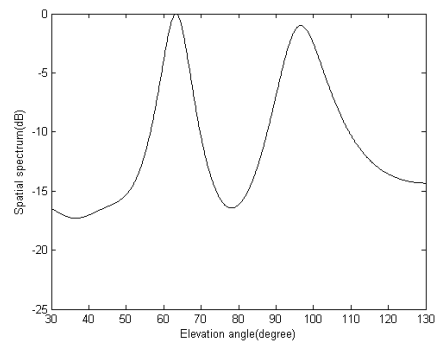


**Figure 21.** The spatial spectrum of elevation angle of the proposed algorithm.

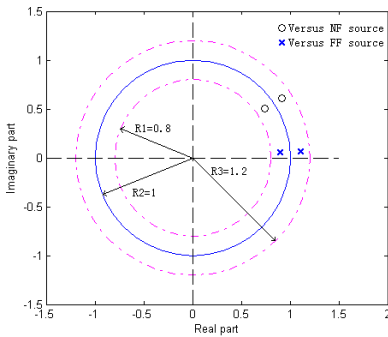


**Figure 22.** The distribution of roots of Equation (27) versus the NF and FF sources.

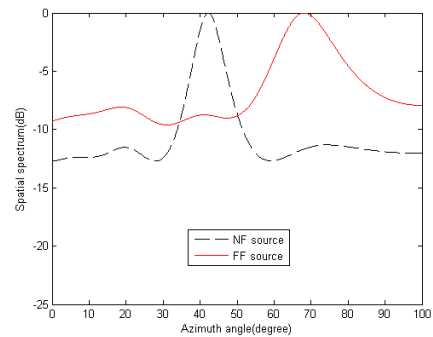


**Figure 23.** The spatial spectrum of azimuth angle of the proposed algorithm.

because the two sound sources are small plane sound sources rather than the ideal point sound sources. Therefore, from the experiment results, we can determine that the proposed algorithm successfully achieves the localization of the mixed sources, and further verifies the validity of the proposed algorithm.

### 5. CONCLUSION

In this paper, based on ESPRIT and MUSIC methods, a mixed sources localization algorithm for mixed 3-D NF and FF sources is proposed. It first utilizes the ULA aligned with the  $Z$  axes which contains 2-D information (elevation angle and range) so as to estimate the elevation angle and range parameters of the mixed NF and FF sources. And then with the estimates of the elevation angle and range parameters, the proposed algorithm uses the ULA aligned with the  $X$  axes which contains 3-D information (elevation azimuth angles and range) to obtain the azimuth angle estimates of all mixed sources. Moreover, under the condition that the elevation angles can be resolved clearly, the proposed algorithm is able to accurately obtain the estimates of the elevation, azimuth angle and range parameters. The proposed algorithm has much better performance than 1-DML algorithm when estimating the elevation angle and range parameters of the NF sources, and approximate performance with 1-DML algorithm when estimating the elevation angle parameters of the FF sources. Besides, the proposed algorithm has low computational burden and does not require parameter pairing procedure.

## ACKNOWLEDGMENT

This work was supported in part by the National Natural Science Foundation of China under Grant 51275349 and 50375110, in part by the China New Century Excellent Talents in funding this project Grant NECT, in part by the China Tianjin Science and Technology to support key projects Grant 11ZCKFGX03600 and in part by the China Tianjin Science and Technology Sea Project Grant KX2010-0006.

## REFERENCES

1. Krim, H. and M. Viberg, "Two decades of array signal processing research: The parametric approach," *IEEE Signal Process. Mag.*, Vol. 13, No. 4, 67–94, 1996.
2. Schmidt, R. O., "Multiple emitter location and signal parameters estimation," *IEEE Trans. on Antennas and Propagation*, Vol. 34, No. 3, 267–280, Mar. 1986.
3. Roy, R. and T. Kailath, "ESPRIT — Estimation of signal parameters via rotational invariance technique," *IEEE Trans. on Acoust., Speech, Signal Processing*, Vol. 37, No. 7, 984–995, Jul. 1989.
4. Gao, F. F. and A. B. Gershman, "A generalized ESPRIT approach to direction-of-arrival estimation," *IEEE Signal Processing Letters*, Vol. 12, No. 3, Mar. 2005.
5. Lizzi, L., F. Viani, M. Benedetti, P. Rocca, and A. Massa, "The M-DSO-ESPRIT method for maximum likelihood DOA estimation," *Progress In Electromagnetics Research*, Vol. 80, 477–497, 2008.
6. Changuel, H., F. Harabi, and A. Gharsallah, "2-L-shape two-dimensional arrival angle estimation with a classical subspace algorithm," *Progress In Electromagnetics Research*, Vol. 66, 301–315, 2006.
7. Yang, P., F. Yang, and Z.-P. Nie, "DOA estimation with sub-array divided technique and interpolated ESPRIT algorithm on a cylindrical conformal array antenna," *Progress In Electromagnetics Research*, Vol. 103, 201–216, 2010.
8. Harabi, F., H. Changuel, and A. Gharsallah, "Direction of arrival estimation method using a 2-L shape arrays antenna," *Progress In Electromagnetics Research*, Vol. 69, 145–160, 2007.
9. Swindlehurst, A. L. and T. Kailath, "Passive direction of arrival and range estimation for near-field sources," *IEEE Spec. Est. and Mod. Workshop*, 123–128, 1988.
10. Huang, Y.-D. and M. Barkat, "Near-field multiple source

- localization by passive sensor array,” *IEEE Trans. on Antennas and Propagation*, Vol. 39, No. 7, 968–975, 1991.
11. Grosicki, E. and K. Abed-Meraim, “A weighted linear prediction method for near-field source localization,” *IEEE Transactions on Signal Processing*, Vol. 53, No. 10, 3651–3660, Oct. 2005.
  12. Liang, J. L. and D. Liu, “Passive localization of near-field sources using cumulant,” *IEEE Sensors Journal*, Vol. 9, No. 8, 953–960, 2009.
  13. Starer, D. and A. Nehorai, “Passive localization of near-field sources by path following,” *IEEE Transactions on Signal Processing*, Vol. 42, No. 3, 677–680, 1994.
  14. Challa, R. N. and S. Shamsunder, “Passive near-field localization of multiple non-Gaussian sources in 3-D using cumulants,” *Signal Process.*, Vol. 65, 39–53, 1998.
  15. Dehghanian, V., M. Okhovvat, and M. Hakkak, “A new interpolation technique for the reconstruction of uniformly spaced samples from non-uniformly spaced ones in plane-rectangular near-field antenna measurements,” *Progress In Electromagnetics Research*, Vol. 72, 47–59, 2007.
  16. Challa, R. N. and S. Shamsunder, “3-D spherical localization of multiple non-Gaussian sources using cumulants,” *8th Sag. Proc. Workshop on SSAP*, 101–104, Corfu, Greece, 1996.
  17. Abed-Meraim, K. and Y. Hua, “3-D near field source localization using second order statistics,” *Conference Record of the Thirty-First Asilomar Conference on Signals, Systems & Computers*, Vol. 2, 1307–1311, 1997.
  18. Lee, C. M., K. S. Yoon, J. H. Lee, and K. K. Lee, “Efficient algorithm for localizing 3-D narrowband multiple sources,” *IEE Proc., Radar Sonar Navig.*, Vol. 148, No. 1, 23–26, 2001.
  19. Yan, W., J.-D. Xu, G. Wei, L. Fu, and H.-B. He, “A fast 3D imaging technique for near-field circular SAR processing,” *Progress In Electromagnetics Research*, Vol. 129, 271–285, 2012.
  20. Lee, J. H., D. H. Park, G. T. Park, and K. K. Lee, “Algebraic path-following algorithm for localising 3-D near-field sources in uniform circular array,” *Electronics Letters*, Vol. 39, No. 7, 1283–1285, 2003.
  21. Liang, J. and D. Liu, “Passive localization of mixed near-field and far-field sources using two-stage music algorithm,” *IEEE Transactions on Signal Processing*, Vol. 58, No. 1, 108–120, Jan. 2010.
  22. He, J., M. N. S. Swamy, and M. O. Ahmad, “Efficient application

- of MUSIC algorithm under the coexistence of far-field and near-field sources,” *IEEE Transactions on Signal Processing*, Vol. 60, No. 4, 2066–2070, 2012.
23. Wang, B., J. J. Liu, and X. Y. Sun, “Mixed sources localization based on sparse signal reconstruction,” *IEEE Signal Processing Letters*, Vol. 19, No. 8, Aug. 2012.
  24. Johnson, R. C., *Antenna Engineering Handbook*, 3rd Edition, 9–12, McGraw-Hill, New York, 1993.
  25. Wax, M. and T. Kailath, “Detection of signals by information theoretic criteria,” *IEEE Trans. on Acoust., Speech, Signal Process.*, Vol. 33, 387–392, Apr. 1985.
  26. Barabell, A. J., “Improving the resolution performance of eigenstructure-based direction-finding algorithms,” *IEEE International Conference on ICASSP’83 Acoustics, Speech, and Signal Processing*, 336–339, Boston, MA, May 1983.
  27. Rao, B. D. and K. V. S. Hari, “Performance analysis of root-music,” *IEEE Trans. on Acoust., Speech, Signal Process.*, Vol. 37, No. 12, 1939–1949, Dec. 1989.
  28. Cheng, S.-C. and K.-C. Lee, “Reducing the array size for DOA estimation by an antenna mode switch technique,” *Progress In Electromagnetics Research*, Vol. 131, 117–134, 2012.
  29. Lie, J. P., B. P. Ng, and C. M. S. See, “Multiple UWB emitters DOA estimation employing time hopping spread spectrum,” *Progress In Electromagnetics Research*, Vol. 78, 83–101, 2008.
  30. Liang, J. and D. Liu, “Two L-shaped array-based 2-D DOAs estimation in the presence of mutual coupling,” *Progress In Electromagnetics Research*, Vol. 112, 273–298, 2011.
  31. Li, Y. and H. Ling “Improved current decomposition in helical antennas using the ESPRIT algorithm,” *Progress In Electromagnetics Research*, Vol. 106, 279–293, 2010.
  32. El Korso, M. N., B. Royer, A. Renaux, and S. Marcos, “Conditional and unconditional Cramér-Rao bounds for near-field source localization,” *IEEE Transactions on Signal Processing*, Vol. 58, No. 5, May 2010.
  33. Stoica, P. and A. Nehorai, “MUSIC, maximum likelihood and Cramér-Rao bound,” *IEEE Trans. on Acoust., Speech, Signal Process.*, Vol. 37, No. 5, 720–741, May 1989.
  34. Liang, J. L., X. J. Zeng, B. J. Ji, J. Y. Zhang, and F. Zhao, “A computationally efficient algorithm for joint range-DOA-frequency estimation of near-field sources,” *Digital Signal Processing*, Vol. 19, No. 4, 596–611, Jul. 2009.